Mathematical model for predicting topographical properties of poly (ε-caprolactone) melt electrospun scaffolds including the effects of temperature and linear transitional speed

Junghyuk Ko, Nima Khadem Mohtaram, Patrick C. Lee, Stephanie M. Willerth, and Martin B.G. Jun

2015

Mathematical model for predicting topographical properties of poly (ε-caprolactone) melt electrospun scaffolds including the effects of temperature and linear transitional speed

Junghyuk Ko[1], Nima Khadem Mohtaram[1], Patrick C. Lee[2], Stephanie M. Willerth[1,3,4], and Martin B.G. Jun[1,*]

[1]Department of Mechanical Engineering, University of Victoria, Victoria, BC, V8W 2Y2, Canada
[2]School of Engineering, University of Vermont, VT, 05405, USA
[3]Division of Medical Science, University of Victoria, BC, V8W 3P6, Canada
[4]Department of Biomedical Engineering, University of Victoria, BC, V8W 3P6, Canada

Abstract

Melt electrospinning can be used to fabricate various fibrous biomaterial scaffolds with a range of mechanical properties and varying topographical properties for different applications such as tissue scaffold and filtration and etc., making it a powerful technique. Engineering the topography of such electrospun microfibers can be easily done by tuning the operational parameters of this process. Recent experimental studies have shown promising results for fabricating various topographies, but there is not that body of work that focuses on using mathematical models of this technique to further understand the effect of operational parameters on these properties of microfiber scaffolds. In this study, we developed a novel mathematical model using numerical simulations to demonstrate the effect of temperature, feed rate and flow rate on controlling topographical properties such as fiber diameter of these spun fibrous scaffolds. These promising modelling results are also compared to our previous and current experimental results. Overall, we show that our novel mathematical model can predict the topographical properties affected by key operational parameters such as change in temperature, flow rate and feed rate and this model could serve as a promising strategy for the controlling of topographical properties of such structures for different applications.

Key words

Melt electrospinning, Modeling, Topography, Microfibers, and Scaffolds.

*To whom correspondence should be addressed. Tel. :(1-250-853-3179); e-mail: mbgjun@uvic.ca

1. Introduction

Electrospinning has gained increasing popularity in recent years due to a surge in research investigating micro and nanoscale fabrication technologies [1-6]. Electrospinning is a manufacturing technique that can produce both nano- and microfiber structures. These techniques can involve both solution and melt electrospinning. Solution electrospinning produces fibers on the nanoscale due to a whipping instability when fibers are stretched out from the spinning solution. The process of melt electrospinning involves melting the polymer of choice before being extruded into fibers. Electrospun scaffolds can be fabricated with similar properties to the extracellular matrix and can thereby support cells adhesion, making it attractive for tissue engineering applications [1, 2, 5, 7-11].. However, control over scaffold topography and porosity is limited because of randomness of the whipping instability. Melt electrospinning gives

precise control over scaffold topography and porosity, but the fibers are on the micro scale [4, 9, 12-17] . This is because the whipping instability stage is absent due to the lower conductivity and higher viscosity of the polymer melt.

Using melt electrospining, a variety of electrospun scaffolds with varied topographies can be produced with a high degree of controllability and reproducibility [3, 4, 9, 10, 18, 19]. Electrospun microfibers present an excellent ability of controlling the topography of scaffolds for several tissue engineering applications in which the effect of physical cues would play a key role in studying cell-scaffold interactions [7, 9]. The fabrication of such scaffolds requires an excellent degree of topographical controllability. Melt electrospining has been used as a powerful technique to achieve the controllability and also the reproducibility of topographical properties including fiber diameter, scaffold architecture, porosity and eventually mechanical properties such as elastic modulus [10, 11, 15, 20-24].

Melt electrospinning is also preferred for biomaterials as there is no use of toxic solvents, unlike solution electrospinning [3, 5, 7, 8, 10]. Melt electrospinning can control the fiber diameter, which can be altered by adjusting parameters such as computer numerical control (CNC) feed speed, extrusion die nozzle diameter, melt temperature, flow rate, and electric field strength [9, 12, 17, 18, 20-22, 24-26]. Also, melt electrospinning allows for higher viscous forces than solution electrospinning, which means that the viscous forces can balance with electric field forces[13]. As a result, the fibers can be drawn out to be thicker than in solution electrospinning. Therefore, melt electrospinning is a sound method for the creation of specific topographies using microfibers [9, 14].

To achieve a scaffold that provides specific mechanical and topographical properties, mathematical models have been developed to predict the effect of key operational parameters such as nozzle size, temperature, collecting distance and applied voltage on controlling the fiber size and porosity [17, 25-27]. Although melt electrospining has shown its promising potential in tissue engineering applications, controlling scaffold topography, however, still remains challenging [9, 14, 20, 21]. Experimentally, many research papers have shown the effects of the fiber diameter, nozzle size and temperature on controlling topographical properties such as fiber diameter and porosity, and there are few mathematical models to promote the understanding of these effects[6, 9, 15, 17, 23-28]. Following our previous work on mathematical modelling of melt electrospining [9, 25], we believe that the understanding of the effects of these parameters on topography is possible and the results would be very helpful for engineers in the field to create microfibers with different morphologies by varying the parameters. In our previous work, the electrospun fiber's properties were fully explained by the geometrical models but scaffold models partially required experimental data to predict microfibers' morphology on counter electrode. Moreover, effects of temperature, flow rate and transitional speed on microfiber's properties were not reflected in our previous models [25].

In this study we will present a validation of our novel geometrical model to predict topographical features of electrospun melt fibers altered by nozzle diameter, applied voltage, collecting distance, and various heating temperatures on radius of helix and microfiber topology. Moreover the effect of various linear transition speeds and flow rates on the microfiber topology will be investigated as well. In addition, overlapped force model is added to demonstrate pulling force each other molten condition's fibers in neighbouring distance. To further understand the effect of operational parameters on the properties of microfiber scaffolds, helix movement and three dimensional scaffold modeling are added in our previous

models in this study. For each set of controlling parameters, numerical results are discussed in detail and compared to the experimental data.

2. Modeling procedure

2.1 *Geometrical modeling*

At the beginning, the extruded polymer melt at the tip of the nozzle is like a truncated spherical droplet which changes its shape after the formation of the electric field. The geometrical models for melt electrospinning process such as Taylor cone and straight jet were established in [25]. Furthermore, the microfiber extruded from droplet was geometrically defined as a funnel as shown in Figure 1. The relation between nozzle radius r_1 and straight jet radius r_2 are calculated by [25]:

$$r_2(t) = \frac{-h_1(t)\pi r_1 \pm \sqrt{3\pi}\sqrt{-4(h_1(t)-3h_2(t))Qt - h_1(t)(h_1(t)-4h_2(t))\pi r_1^2}}{2(h_1(t)-3h_2(t)\pi)} \quad (1)$$

where, Q is flow rate. In the beginning the height of droplet $h_0 = r_1$, the radius of the nozzle which is constant. After the introduction of electrical force polymer melt move toward counter electrode the height of the jet changes with time. Therefore height of Taylor cone h_1 and straight jet h_2 can be can be defined as [25]:

$$h_n(t) = h_{n-1} + \int_0^t u_n(t)dt \quad (2)$$

where, $n = 1,2$, and $u(t)$, the electrospinning velocity at any time t is calculated by [25]:

$$u_n(t) = u_{n-1} + \int_0^t \frac{\sum F}{m} dt \quad (3)$$

where, $n = 1,2$ represent Taylor cone and straight jet respectively, $\sum F$ is the sum of forces; surface tension F_s, viscoelastic F_v, gravity F_g, microfiber tension F_T and electrostatic F_e, and m the mass of polymer melt which are discussed in next sections.

2.2 The forces associated with the straight jet

The forces associated with the straight jet are surface tension (F_s), viscoelastic (F_v), gravity (F_g), and electrostatic (F_e). The surface tension force (F_s) is given in [25] as:

$$F_s = \frac{-\gamma\left(\mathrm{a}_{s_{n+1}}(t) - \mathrm{a}_{s_n}\right)}{h_n(t)} \quad (4)$$

where, surface tension γ, which is by definition work per change in surface area is given as $\gamma = \int \frac{2\,F_s r\,h_n(t)}{\mathrm{a}_{s_n}}$ and $\mathrm{a}_{s_1}(t) = \pi\big(r_1 + r(t)\big)\sqrt{\big(r_1 - r(t)\big)^2 + (h(t))^2}$, $a_{s_2}(t) = 2\pi r(t)(r(t) + h(t))$ are surface area of Taylor cone and straight jet respectively at $n = 1,2$.

The molten PCL polymer exhibited both viscous and elastic characteristics during electrospinning process. The viscoelastic force F_v is calculated by:

$$F_v = -\sigma(t)A \quad (5)$$

where, A is the area of the jet top and the corresponding stress $\sigma(t)$ can be demonstrated through the relationship, $\sigma = Y\varepsilon + \eta_d\dot{\varepsilon}$. Strain $\varepsilon$and strain rate $\dot{\varepsilon}$, fiber deformation from Taylor cone, can be defined with $\varepsilon = \frac{h + \int_0^t u_n dt - 2\pi(\frac{1}{3}r + \frac{2}{3}r_1)}{\frac{4tQ}{2\pi(\frac{1}{3}r + \frac{2}{3}r_1)}}$ and $\dot{\varepsilon} = \frac{d\varepsilon}{dt}$, where Young's modulus Y and dynamic viscosity $\eta_d = e^{-\frac{E_n}{RT}}$ (E_n:activation energy, R: gas constants) [25].

The gravity force and electrical force that act in the same direction of the flow the jet are calculated by:

$$F_g(t) = mDg \tag{6}$$

$$F_e(t) = \frac{e(t)\psi}{z} \tag{7}$$

where, the density D of the material(PCL)[9], the jet mass m at time t , and the charge on the jet $e(t)$ [29] are given as :

$$D = \frac{0{\cdot}9049\, e^{0.0006392T}}{0.99868+0.0081076T+0.000070243T^2} \qquad 80\,^{\circ}\text{C} \le \text{T} \le 150\,^{\circ}\text{C} \tag{8}$$

$$e(t) = 8\pi\sqrt{r_2^2(t)\,\gamma\varepsilon_o C} \tag{9}$$

where, ε_o, C, ψ , z are respectively permittivity of vacuum, feasibility factor of material, applied voltage and the counter electrode distance from the tip of nozzle [25].

Energy Equation is defined by Eq. (10)

$$\frac{dT}{dz} = -\frac{2\pi r_2 h_t(T-T_a)}{QC_p} \tag{10}$$

where, C_p is specific heat for polymer which is given in Table 1, h_t heat transfer coefficient, T and T_a the polymer fiber temperature and ambient temperature (˚C).

Further, we have derived the expression for the correlation of temperature and fiber diameter using Eq. (11) as [29]:

$$h_t = \frac{k}{2r_2}\left[0.42\left(\frac{2r_2u}{v}\right)^{0.334}\left(1+\frac{8v}{u}\right)^{0.167}\right] \tag{11}$$

$$v = \frac{4Q}{\pi r_2^2 DC_p} \tag{12}$$

where, *k, Q, v* and *u* are respectively conductivity, flow rate, cooling air velocity and fiber velocity.

2.3 Helix movement modeling

The extruded microfibers from nozzle are passed through electromagnetic field when high voltage is applied between nozzle and counter electrode. The combination of electric and magnetic forces is Lorentz force on a point charge. Thereby the fibers have helix movements until reaching counter electrode. Figure 2 shows schematic of Lorentz force (F_L) in melt electrospinning. The Lorentz force (F_L) calculated by:

$$\overrightarrow{F_L} = q \times \left(\vec{E} + \vec{V} \times \vec{B}\right) \tag{13}$$

$$\vec{E} = \frac{k_e q}{z^2}\overrightarrow{u_r}, \vec{V} = \frac{P}{Me}, \vec{B} = \frac{\mu_0 I}{4\pi}\int_0^l \frac{d\vec{l}\times\hat{r}}{r^2} \tag{14}$$

where, *E, q,* $\overrightarrow{u_r}$*, P, Me,* μ_0*, I, l,* k_e*, r* are respectively electric field intense, charge, the unitary vector in the direction of the electric field, momentum of electron, mass of electron, magnetic constant, current, length of wire, electric field coefficient, and distance from wire, which are given in Table 1.

2.4 Three dimensional (3D) scaffold modeling

The topology of scaffold is determined by radius of helix movement (R), linear transitional speed (v_L), and overlapped force (F_o) including fiber radius (r_2) and fiber velocity (v) calculated from the previous sections. Figure 3A shows a schematic of helix movement on flat surface as a substrate. The acceleration of the electrospun fibers on the substrate is equal to the sum of the forces on the fibers divided by mass of the microfibers according to Newton's second law and we assume the initial displacement is close to zero. Therefore, the radius of helix movement (R) is defined by:

$$R(t) = \int_0^{t_e}\int_0^{t_e} \frac{F_L cos\theta_1 - (F_T + F_o)}{m(t)}\, dt\, dt \tag{15}$$

$$F_T = F_{T1}sin\theta_2 + F_{T2}, F_{T1} = F_s + F_v + F_g + F_e, F_{T2} = \mu_1 m(t_e)g + m\frac{v_L}{dt} \quad (16)$$

$$m(t) = \pi r_2^2(t) l_L D(t) \quad (17)$$

$$t_e = \frac{z}{u(t)} \quad (18)$$

where, m(t) is mass of microfiber, tension force (F_T) on flat surface has two components which are F_{T1} and F_{T2}, t_e is microfiber's reaching time to counter electrode after straight jet, l_L is fiber length applied Lorentz force, and μ_1 is friction constant of aluminum foil which is given in Table 1.

Figure 4 shows topology of microfibers using 300μm nozzle, 20kV voltage, and 5cm distance in melt electrospinning. The microfibers in Figure 4(A) have loop patterns in melt electrospinning because of Lorentz force. In the meantime, overlapped force (F_o) is happened among fibers, which is a pulling force each other molten condition's fibers in adjacent distance. The overlapped force (F_o) is calculated by [17]:

$$F_o = \frac{1}{4\pi\varepsilon_0}\frac{q}{a(t)^2},\ T \geq T_m \quad (19)$$

where, a(t), T, T_m,ε_0 are respectively the adjacent distance of electrospun microfibers, polymer fiber temperature calculated by Eq. (10), melt temperature, and permittivity of vacuum. Figure 4(B) demonstrates the results of the overlapped force applied (solid line) and non-applied (dash line).

Figure 3B demonstrates a schematic of helix movement on round surface as a substrate. Tension force (F_T) on round surface is calculated by sum of three components:

$$F_T = F_{T1}cos\theta_2 + F_{T2} + F_{T3} \quad (20)$$

$$T_1 = F_s + F_v + F_g + F_e, T_2 = \mu_1 m(t_e)g + m\frac{v_L}{dt}, T_3 = \mu_1 m(t_e)g + m\frac{2\pi R_D \alpha}{dt} \quad (21)$$

where, α, and R_D are respectively drum angular velocity and drum radius. The radius of helix movement in case of round surface can be acquired as substituting the tension force to Eq. (15).
The porosity of fabricated scaffold ($\emptyset_{mesh}$) is defined by[25]:

$$\emptyset_{mesh} = \left(1 - \frac{\pi r_2^2 \int u dt}{V_s}\right) \times 100\ \% \quad (22)$$

where, V_s is volume of whole scaffold.

3. Experimental procedure

3.1 Fabrication of microfibers

Poly (ε-caprolactone) (PCL,Mn ~45,000) was acquired from (Sigma Aldrich, USA) with a melting point of approximately 60°C. The details of our custom-made melt electrospinning setup have been already published [9, 25]. In summary, we have applied 10kV to 20kV to the molten PCL at 80˚C using a high voltage power supply (Gamma High Voltage Research Inc., USA) with the working distance between the nozzle and counter electrode ranging from 5cm to 20cm. The PCL granules were heated to the desired temperature after the granules were dispensed into melting chamber with the nozzle attached. To our knowledge, parameters such as nozzle diameter, processing temperature, collection distance, applied voltage, flow rate of syringe pump and linear velocity of x and y axis in CNC machine are related to fiber diameter and morphology of scaffold in melt electrospinning. The influence of electrical force (F_e), nozzle diameter (r_1), counter electrode distance (z), porosity of scaffold ($\emptyset_{mesh}$) and linear velocity (v_L) in morphology of scaffold were investigated in numerical simulation and experiment [25].

3.2 Analysis of microfiber topography

To image these scaffolds using scanning electron microscopy (SEM), all electrospun microfibers were coated using Cressington 208 carbon coater two times for 6 seconds at 10^{-4} *m*bar and accordingly samples were transported to loading stubs for Hitachi S-4800 field emission scanning electron microscope. Low magnification images were captured at 1 kV with approximately 8 mm working distance. Fiber diameters and radius of helix were characterized by Quartz-PCI Image Management Systems® [25].

4. Parameter analysis in numerical simulation

4.1 Parameters study depended on various temperatures

The influence of temperature on the other melt electrospinning parameters (density of PCL, viscoelastic force, electrospinning speed, fiber diameter) was examined by simulation. The applied voltage, distance between nozzle and counter electrode, flow rate, linear transitional speed, and nozzle diameter are fixed all respectively at 20kV, 5cm, 2ml/h, 8.5mm/s, and 300μm in order to restrict the parameters effects. Viscosity and density of PCL polymer strongly depends on temperature and it eventually influences to viscoelastic force, electrospinning speed, and fiber diameter as shown in Figure. 5. The density of PCL is changed from 0.7957 (g/cm^3) to 0.3440 (g/cm^3) when the temperature is changed from 80 ˚C to 150 ˚C in Figure 5(A). Figure 5(B) shows increases of viscoelastic force in higher temperature. Electrospinning velocity (u) is increased from approximately 100mm/s to 180 mm/s because of low viscosity resulted from temperature as shown in Figure 5(C). As the results, the fiber diameter is decreased by approximately 0.020mm when temperature is varied from 80 ˚C to 150 ˚C as shown in Figure 5(D).

4.2 Parameters study depended on various linear transitional speed

Figure 6 shows the effects of various linear transitional speeds on the resulting tension force and radius of helix. To limit the other parameters effects, the applied voltage, distance between nozzle and counter electrode, flow rate, temperature and nozzle diameter are fixed all respectively at 20kV, 5cm, 2ml/h, 80 ˚C, and 300μm. Figure 6(A) demonstrates tension force in various transitional speeds on flat surface counter electrode. The tension force influenced on electrospun microfibers is changed from approximately 0.04N to 0.09N when the speed is varied from 8mm/s to 20mm/s. According to Eq. (15), the radius of helix is inversely proportional to the linear transitional speed as shown in Figure 6(B) so it is changed from 0.55mm to 0.31mm when the linear transitional speed is varied from 8mm/s to 20mm/s.

4.3 Parameters study depended on various flow rates

The flow rate of melt PCL affects the volume of the system at any time so the parameter makes changes in electrical force, tension force, gravity force, Lorentz force, electrospinning speed, and radius of helix as shown in Figure 7. The other parameters (the applied voltage, distance between nozzle and counter electrode, temperature, linear transitional speed and nozzle diameter) are respectively fixed at 20kV, 5cm, 80 ˚C, 8.5mm/s and 300μm in order to study effect of the flow rate. Electrical force shows decrement of 2.7% since surface tension is increased, tension force presents decrement of 3.7% because the electrical force is decreased, gravity force demonstrates increment of 11% since the amount of PCL is increased, and Lorentz force displays decrement of 2.9% because the gravity force is increased when flow rate is increased from 2ml/h to 10ml/h as shown in Figure 7(A-D) and initial volume increased by higher flow rate is increasing electrospinning velocity as presented in Figure 7(E) and thereby the radius of helix is

decreased by approximately 0.030mm since Lorentz force is decreased when the flow rate is changed from 2ml/h to 10ml/h as shown in Figure 7(F).

4.4 Effects of nozzle diameter, applied voltage, distance, and linear transition speed in various temperatures

In our previous paper [25], we compared numerical and experimental results and confirmed our modeling to be reliable at 80 ˚C. The predictions of fiber diameter and porosity under ambiguous parameters including various temperatures are shown in Figure 8, with conditions (20kV applied voltage, 5cm distance, and 2ml/h flow rate). The fiber diameter replied on the diameter of the nozzle and it shows linear proportional to the nozzle diameters and proportional to the diameters in various temperatures as well. However, the proportional ratio is slightly decreased when the temperature is increased from 80 ˚C to 150 ˚C as shown in Figure 8 (A). We can expect that distance and applied voltage have an inverse relationship according to Coulomb's law and influence fiber diameter inversely as well. Moreover, the curves of 100 ˚C to 150 ˚C in temperature have similarity with the curves of 80 ˚C but they are overall shifted down as shown in Figure 8 (B) and (C). Figure 8 (D) shows porosity of scaffolds depended on various temperatures. The porosity of microfibers in 80 ˚C shows 83% when the transitional speed is 8.5mm/s while the porosity in 150 ˚C demonstrates 91% when the speed is 8.5mm/s. The faster convergence to approximately 90 % porosity is at higher temperature. In addition, Figure 9 (A: 80˚C) and (B: 120˚C) presents effects of temperature and linear transitional speed in porosity prediction at 200μm nozzle diameter, 20kV applied voltage and 5cm distance. The current model is able to predict porosity within average 5.5% difference from experimental results while the previous model[25] was able to predict porosity within average 10.2% difference.

5. Numerical simulation and experimental results

5.1 Effect of Temperature influenced on fiber diameter and radius of helix

The effect of temperature on the fiber diameter and radius of helix is studied by simulation and experiment. The simulation and experiment are conducted under the same conditions which are 300μm nozzle, 5cm distance, 20kV voltage, 2ml/h flow rate, and 8.5mm/s transitional speed. Figure 10 (A) and (B) present a comparison of numerical and experimental fiber diameter and radius of helix for various temperatures. The increase in temperature would eventually affect viscoelastic force and density to stretch out fibers according to Eq. (5) and (8). Experimentally, that eventually would lead to the fiber diameter decreasing from 0.041 ± 0.008 to 0.028 ± 0.005 mm (n=5) as the temperature increases from 80˚C to 150 ˚C. In simulation, the fiber diameter decreased from 0.034 to 0.030 mm as the temperature increased from 80˚C to 150 ˚C. Moreover, radius of helix decreases from 0.52 to 0.43mm in the simulation. Experimental radius of helix in Figure 10 (B) is varied from 0.64 ± 0.17to 0.42±0.11mm (n=5) when temperature is increased from 80˚C to 150 ˚C.

5.2 3D tubular scaffold topology controlled by linear transitional speed

The transitional speed (v_L) in scaffold modeling is a significant parameter to define the topology of controlled tubular scaffolds. Figure 11 shows that (8 mm × 100mm) (inner diameter × length) numerical and experimental topology depended on various transitional speeds at 300μm (nozzle diameter), 20kV (applied voltage), 5cm (distance), 80˚C (temperature), 1.04 rad/s (angular velocity), and 2ml/h (flow rate). (A), (B), and (C) in Figure 11 respectively represent 4.25mm/s, 8.50mm/s, and 17.00mm/s transitional

speed. The rolling angle of microfibers on round substrate shows respectively 56˚, 42˚, and 23˚ at 4.25mm/s, 8.50mm/s, and 17.00mm/s in experimental data. In numerical simulation, the angle shows respectively 55˚, 42˚, and 22˚ at the same transitional speed. If v_L is increased, the radius of helix (R(t)) is decreased since tension force (F_T) on microfibers is increased. The intervals between tori thereby become sparser when transitional speed is increased.

6. Discussion

Using numerical simulations, the effect of temperature on controlling topographical properties was also studied by investigating the effect of temperature on density, viscoelastic force, electrospinning speed and also fiber diameter. Mathematical modelling approaches can be used to predict the topographical dependency of microfiber scaffolds on various operational parameters for better understanding of melt electrospinning technique through the use of numerical studies and comparing the results with experimental data [17, 22, 25, 26]. We have previously shown that the topographical properties of melt eletcrsopun scaffolds had directed stem cell differentiation into neural phenotypes [9]. Thus, a trustworthy approach such as mathematical modelling must be used to control topographical properties [24, 25]. The topographical properties have been previously shown to be drastically affected by several operational parameters [6, 13, 15, 17, 22, 24, 25, 27, 28]. However, here we reported the dependency of helix movement on electric and magnetic forces. In addition, 3D modelling was done to study the behaviour of helix movement and linear transitional speed.

In order to produce an effective model to further predict the key topographical properties such fiber diameter and porosity [17, 22, 24, 26], it was necessary to study the effect of nozzle diameter and voltage on fiber diameter. We also studied the impression of distance on fiber diameter. Moreover, the porosity of such scaffolds was shown to be strongly affected by linear transitional speed. We could successfully study these effects while varying temperature from 80˚C to 150˚C as well. Among many studies, we believe that our previous and current models could be introduced as one of the most commonly applicable models for controlling topographical properties which are needed in neural tissue engineering applications. However, our numerical models need to have boundary conditions in nozzle diameter, applied voltage, distance, transitional speed and temperature since our models may not be applied in cases of extreme operational parameters. For example, fiber diameter doesn't be influenced by extremely large nozzle diameter in practical experiment but it is slightly changed in numerical simulation. It may result in extremely high viscoelastic and surface tension force. The fiber diameter was also reported to be drastically changed by altering the applied voltage and distance. However, it is difficult to predict fiber diameter due to short circuit when voltage is extremely high or distance is extremely low. Moreover, porosity of fibrous scaffolds showed a strong dependency transition speed but it is challengeable to calculate the porosity because our models exclude PCL tensile property model. Finally, temperature could significantly change the micro scale topography properties such as fiber diameter and helix radius. However, it is very tough to expect the topography properties in extremely high temperature because of characterization of the ignition behavior of PCL.

In this study, we successfully established comprehensive models to enhance its feature to control the topographical properties of melt electrospun fibrous scaffolds. Our mathematical model can be used to investigate the effects of different key parameters such as temperature, feed rate, flow rate, fiber diameter

and porosity. Such flexibility makes this model attractive for tissue engineers and their desired applications. We have chosen PCL, a commonly used biodegradable polymer which is tailorable in its mechanical properties, rate of surface and bulk biodegradation, solubility and crystallinity, and structure topography[9]. We have also evaluated the performance of such model to investigate the topographical properties of tubular scaffolds which can be used for nerve tissue engineering approaches especially for peripheral nerve injures. On-going work is investigating the effects of viscoelastic properties of polymer melt and also its molecular weight on controlling the topographical properties of melt electrospun fibrous scaffolds to further our current mathematical model.

7. Conclusion

Here we aimed to predict the effect of linear transitional speed on most important forced involved in the melt electrospun process. These forces include tension forces, electrical forces, Lorentz force and also gravity forces. The dependency of such forces on linear transitional speed was studied. The effect of flow rate was also considered to further investigate the effect of these forces along the change in radius of helix as one of the most important topographical properties of such scaffolds. The aim of this research is to add helix movement modeling and three dimensional scaffold modeling to our previous models to predict radius of helix and topography of scaffold incorporating nozzle size, counter electrode distance, applied voltage, temperature, linear transitional speed, and flow rate. Experimentally elusive variable effects are demonstrated through numerical simulations at the fixed conditions.

- Density of PCL shows decrease of 57%, viscoelastic force presents increase of 250%, electrospinning velocity demonstrates increase of 80% and fiber diameter displays decrease of 8% when temperature is increased from 80˚C to 150˚C while fixing all other variables.
- Tension force presents increase of 125% and radius of helix shows decrease of 36% when linear transitional speed is varied from 8mm/s to 20mm/s.
- Electrical force shows decrease of 2.7%, tension force presents decrease of 3.7%, gravity force demonstrates increase of 11%, and Lorentz force displays decrease of 2.9% when flow rate is increased from 2ml/h to 10ml/h.
- The effect of temperature on the fiber diameter was evaluated and the simulation results are compared with experimental data. The fiber diameter presents decrease of 32% when the temperature increases from 80˚C to 150 ˚C. In simulation, the fiber diameter demonstrates decrease of 12% as the temperature increased from 80˚C to 150˚C. Moreover, radius of helix shows decrease of 17% in the simulation. Experimental radius of helix presents decrease of 34% when temperature is increased from 80˚C to 150 ˚C.
- Morphology of tubular scaffold is controlled by linear transitional speed. The rolling angle of microfiber on the round substrate presents respectively decrease of 60% and 59% and in simulation and experiment when the linear transitional speed is changed from 8.5mm/s to 17mm/s. In addition, the fabricated tubular scaffold becomes sparser in the faster transitional speed in both simulation and experiment.

The reliable mathematical modeling enabled to predict and design morphology under various parameters holds great promise for specific scaffold fabrication.

Acknowledgment

Funding support from Natural Sciences and Engineering Research Council (NSERC) Discovery Grants is acknowledged. The authors would also like to acknowledge the Advanced Microscopy Facility at the University of Victoria.

References

1. Mohtaram, N.K., A. Montgomery, and S.M. Willerth, Biomaterial-based drug delivery systems for the controlled release of neurotrophic factors. *Biomedical materials*, 2013. **8**(2): p. 022001.
2. Chung, S., Ingle, N.P., Montero, G.A., Kim, S.H., King M.W., Bioresorbable elastomeric vascular tissue engineering scaffolds via melt spinning and electrospinning. *Acta Biomaterialia*, 2010. **6**(6): p. 1958-67.
3. Park, S.H., Kim, T.G., Kim, H.C., Yang, D.Y., Park T.G., Development of dual scale scaffolds via direct polymer melt deposition and electrospinning for applications in tissue regeneration. *Acta Biomaterialia*, 2008. **4**(5): p. 1198-1207.
4. Brown, T.D., Dalton, P.D., and Hutmacher, D.W., Direct Writing By Way of Melt Electrospinning. *Advanced Materials*, 2011. **23**(47): p. 5651-5657.
5. Nagy, Z.K., Balogh, A., Dravavolgy G., Ferguson, J., Pataki, H., Vajna, B., and Marosi, G., Solvent-free melt electrospinning for preparation of fast dissolving drug delivery system and comparison with solvent-based electrospun and melt extruded systems. *Journal of Pharmaceutical Sciences*, 2013. **102**(2): p. 508-517.
6. Zhou, H.J., Green, T.B., and Joo, Y.L., The thermal effects on electrospinning of polylactic acid melts. *Polymer*, 2006. **47**(21): p. 7497-7505.
7. Farrugia, B.L., Brown, T.D., Upton, Z., Hutmacher, D.W., Dalton, P.D., and Dargaville, T.R., Dermal fibroblast infiltration of poly(epsilon-caprolactone) scaffolds fabricated by melt electrospinning in a direct writing mode. *Biofabrication*, 2013. **5**(2).
8. Karchin, A., Simonovsky, F.I., Ratner, B.D., and Sanders, J.E., Melt electrospinning of biodegradable polyurethane scaffolds. *Acta Biomaterialia*, 2011. **7**(9): p. 3277-3284.
9. Ko, J., Mohtaram, N.K., Ahmed, F., Montgomery, A., Carlson, M., Lee, P.C., Willerth, S.M., and Jun, M.B.G., Fabrication of poly (-caprolactone) microfiber scaffolds with varying topography and mechanical properties for stem cell-based tissue engineering applications. *Journal of biomaterials science. Polymer edition*, 2014. **25**(1): p. 1-17.
10. Mazalevska, O., Struszczyk, M.H., and Krucinska, I., Design of vascular prostheses by melt electrospinning-structural characterizations. *Journal of Applied Polymer Science*, 2013. **129**(2): p. 779-792.
11. Ren, J., Blackwood, K.A., Doustgani, A., Poh, P.P., Steck, R., Stevens, M.M., and Woodruff, M.A., Melt-electrospun polycaprolactone strontium-substituted bioactive glass scaffolds for bone regeneration. *Journal of biomedical materials research.* Part A, 2014. **102**(9): p. 3140-53.
12. Brown, T.D., Slotosch, A., Thibaudeau, L., Taubenberger, A., Loessner, D., Vaquette, C., Dalton, P.D., Design and Fabrication of Tubular Scaffolds via Direct Writing in a Melt Electrospinning Mode. *Biointerphases*, 2012. **7**(1-4).
13. Dalton, P.D., Grafahrend, D., Klinkhammer, K., Klee, D., and Moller, M., Electrospinning of polymer melts: Phenomenological observations. *Polymer*, 2007. **48**(23): p. 6823-6833.
14. Dalton, P.D., Klinkhammer, K., Salber, J., Klee, D., and Moller, M., Direct in vitro electrospinning with polymer melts. *Biomacromolecules*, 2006. **7**(3): p. 686-690.
15. Hao, M.F., Liu, Y., He, X.T., Ding, Y.M., and Yang, W.M., Factors influencing diameter of polypropylene fiber in melt electrospinning. *Advanced Polymer Science and Engineering*, 2011. **221**: p. 129-134.
16. Li, X.Y., Liu, H., Wang, J., and Li, C., Preparation and characterization of poly(epsilon-caprolactone) nonwoven mats via melt electrospinning. *Polymer*, 2012. **53**(1): p. 248-253.
17. Lyons, J., Li, C., and Ko, F., Melt-electrospinning part I: processing parameters and geometric properties. *Polymer*, 2004. **45**(22): p. 7597-7603.

18. Hao, M.F., Liu, Y., He, X.T., Xie, P.C., and Yang, W.M., Experimental study of melt electrospinning in parallel electrical field. *Advanced Polymer Science and Engineering*, 2011. **221**: p. 111-116.
19. Mota, C., Puppi, D., Gazzarri, M., Bartolo, P., and Chiellini, F., Melt electrospinning writing of three-dimensional star poly(E-caprolactone) scaffolds. *Polymer International*, 2013. **62**(6): p. 893-900.
20. Dalton, P.D., Calvet, J.L., Mourran, A., Klee, D., and Moller, M., Melt electrospinning of poly-(ethylene glycol-block-epsilon-caprolactone). *Biotechnology journal*, 2006. **1**(9): p. 998-1006.
21. Deng, R.J., Liu, Y., Ding, Y., Xie, P., Luo, L, and Yang, W., Melt Electrospinning of Low-Density Polyethylene Having a Low-Melt Flow Index. *Journal of Applied Polymer Science*, 2009. **114**(1): p. 166-175.
22. Kong, C.S., Jo, K.J., Jo, N.K., and Kim, H.S., Effects of the Spin Line Temperature Profile and Melt Index of Poly(propylene) on Melt-Electrospinning. *Polymer Engineering and Science*, 2009. **49**(2): p. 391-396.
23. Nayak, R., Padhye, R., Kyratzis, I.L., and Truong, Y.B., Effect of viscosity and electrical conductivity on the morphology and fiber diameter in melt electrospinning of polypropylene. *Textile Research Journal*, 2013. **83**(6): p. 606-617.
24. Wang, X.N., Xu, Y., Wei, Q.F., and Cai, Y.B., Study on Technological Parameters Effecting on Fiber Diameter of Melt Electrospinning. *Advanced Textile Materials*, 2011. **332-334**: p. 1550-1556.
25. Ko, J., Sukhwinder, B.S., Mohtaram, N.K., Willerth, S.M., Jun, M.B.G., Using mathematical modeling to control topographical properties of poly (ε-caprolactone) melt electrospun scaffolds. *Journal of Micromechanics and Microengineering*, 2014. **24**(6) 065009.
26. Zhmayev, E., Cho, D., and Joo, Y.L., Modeling of melt electrospinning for semi-crystalline polymers. *Polymer*, 2010. **51**(1): p. 274-290.
27. Zhrnayev, E., Zhou, H., and Joo, Y.L., Modeling of non-isothermal polymer jets in melt electrospinning. *Journal of Non-Newtonian Fluid Mechanics*, 2008. **153**(2-3): p. 95-108.
28. Liu, Y., Li, X.H., and Ramakrishna, S., Melt Electrospinning in a Parallel Electric Field. *Journal of Polymer Science Part B-Polymer Physics*, 2014. **52**(14): p. 946-952.
29. Raleigh, X.L., in Dublin Philosophy1884, Edinburgh: London. p. 184.

Table1. Parameters used for numerical simulations

Parameters	Literature and Standard data
Conductivity (*k*)	0.132
Electric field coefficient ($\boldsymbol{k_e}$) **[28]**	$9.0 \times 10^9 Nm^2/c^2$
Momentum of Electron (*P*)	1.03434×10^{-11}kgm/s
Mass of electron (*Me*)	$9.10938291 \times 10^{-31}$
Magnetic constant ($\boldsymbol{\mu_0}$) **[28]**	$4\pi \times 10^{-7}\ N/A^2$
Specific heat for PCL polymer ($\boldsymbol{C_p}$) **[25]**	$(0.3 + 6 \times 10^{-4}T) \times 4 \times 182 \times 10^7$
Flow rate (*Q*)	2ml/h
Activation energy, ($\boldsymbol{E_n}$)	10.1 kcal/mol
Gas constant, (*R*)	1.9872 cal/K·mol
Friction constant ($\boldsymbol{\mu_1}$) of aluminum foil	0.61
Permittivity of vacuum ($\boldsymbol{\varepsilon_0}$) **[29]**	$8.854187817 \times 10^{-12} F/m$
Melt temperature ($\boldsymbol{T_m}$)	60˚C
Ambient temperature ($\boldsymbol{T_a}$)	20˚C

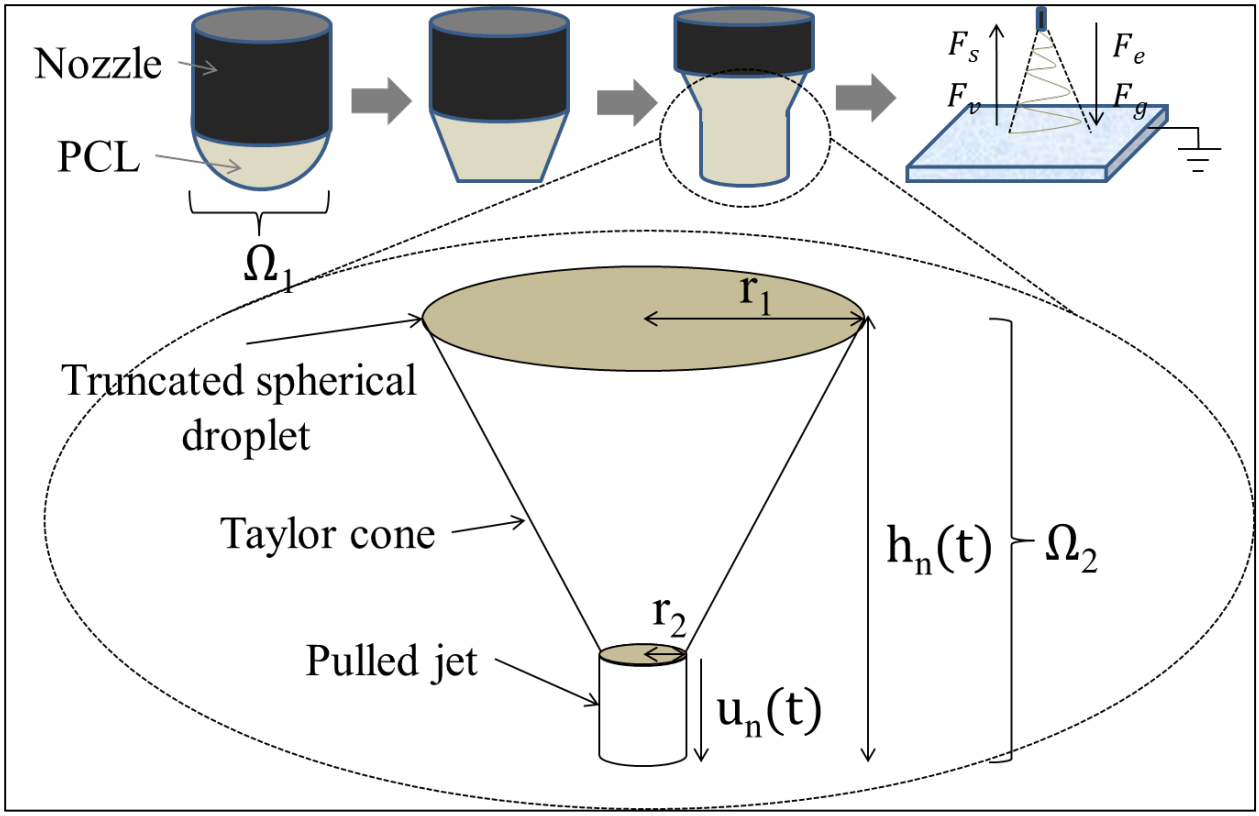

Figure 1. Geometry of different stages of electrospun fiber and the straight jet surmounted by a truncated cone [25]

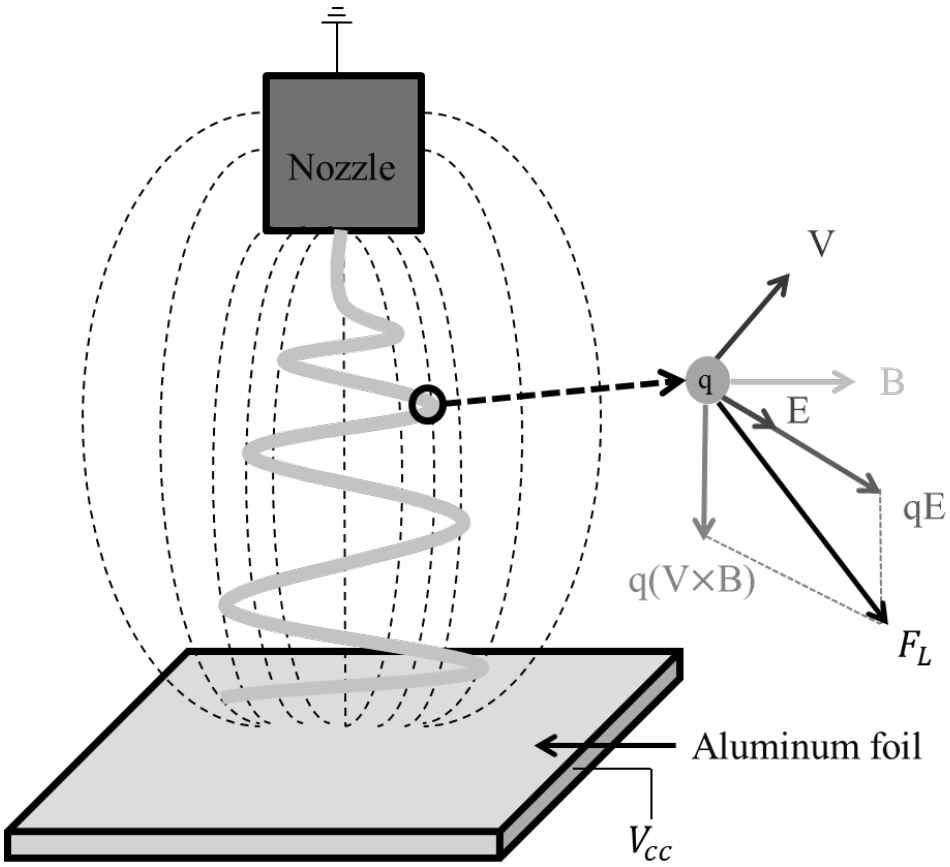

Figure 2. Schematic of Lorentz force in melt electrospinning (E: electric field, V: velocity of electron, B: magnetic field)

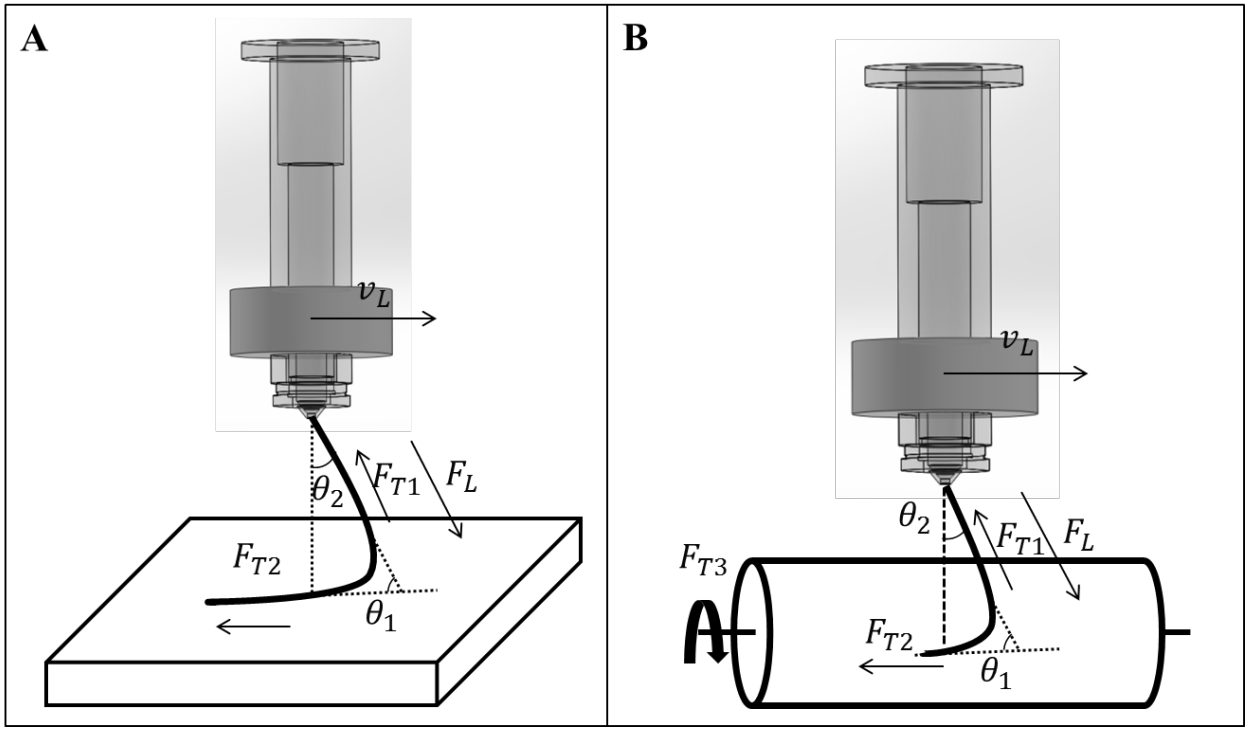

Figure 3 Schematic of helix movement on (A) flat surface and (B) round surface

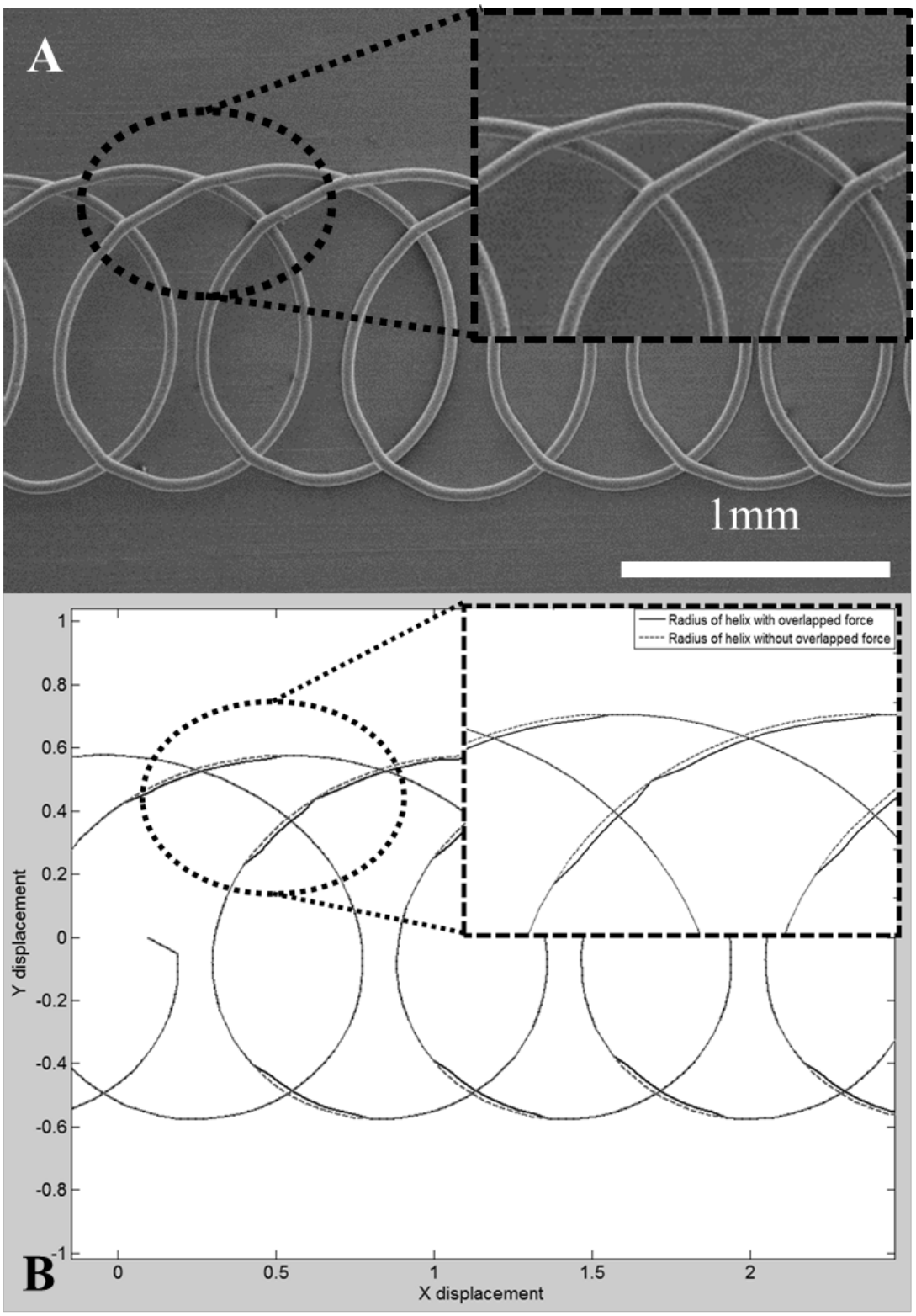

Figure 4. Topology of microfibers using 300 μm nozzle, 20kV voltage, and 5cm distance; (A) Experiment, (B) Simulation.

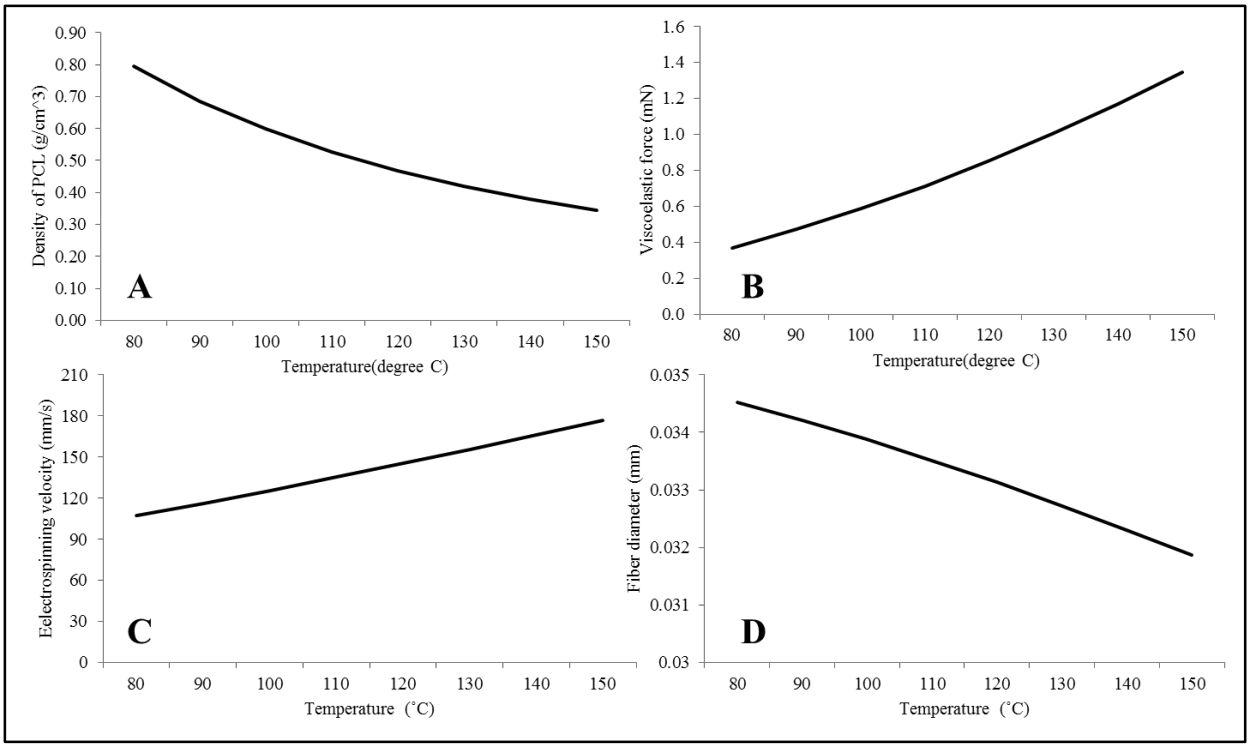

Figure 5. Parameters variation in various temperatures.

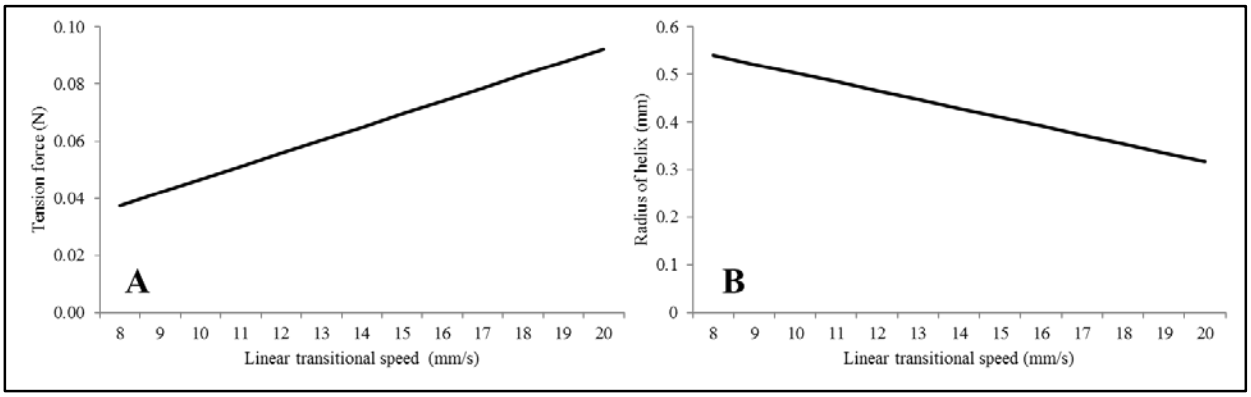

Figure 6. Parameters variation in various feed rate.

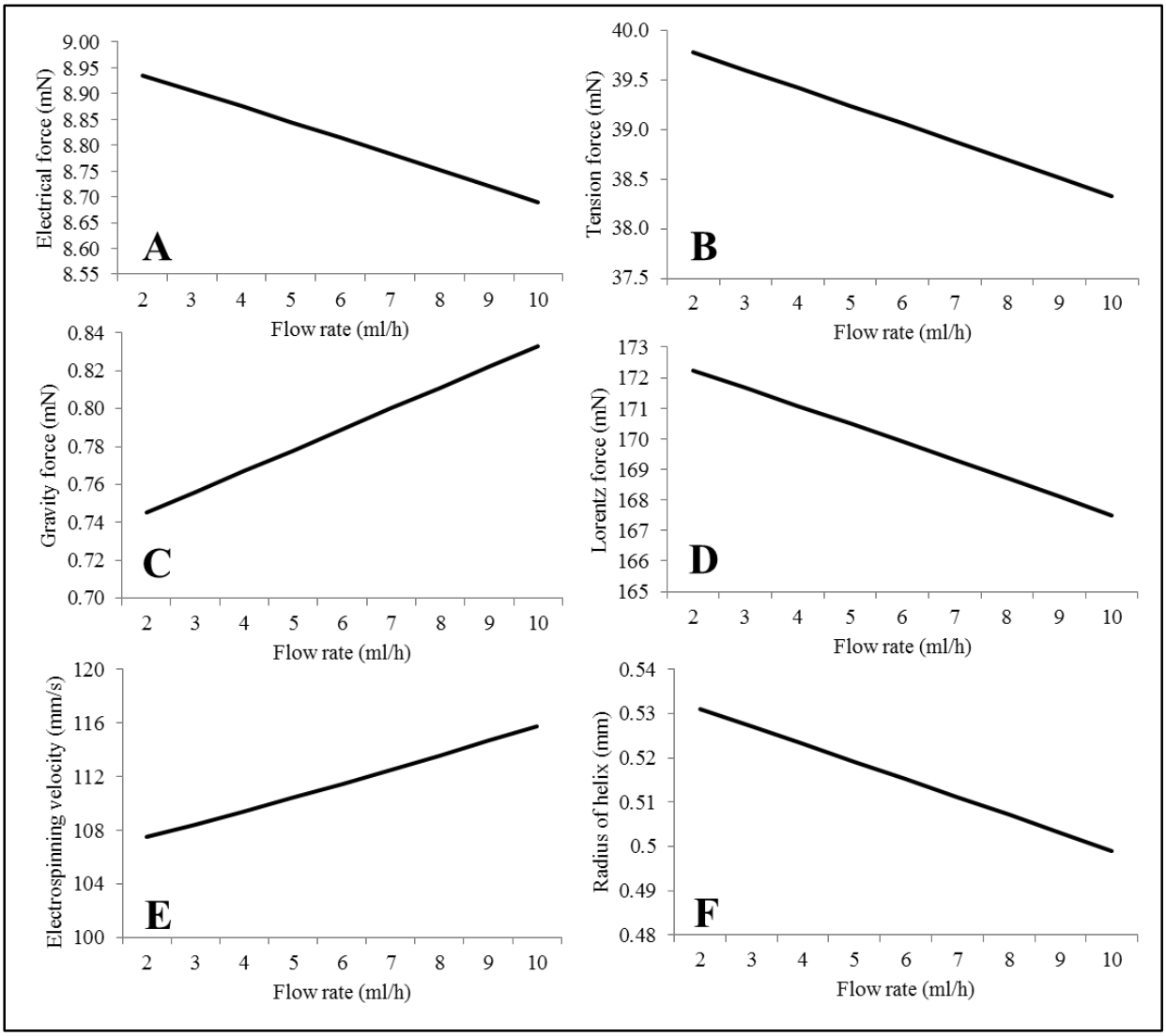

Figure 7. Parameters variation in various flow rate.

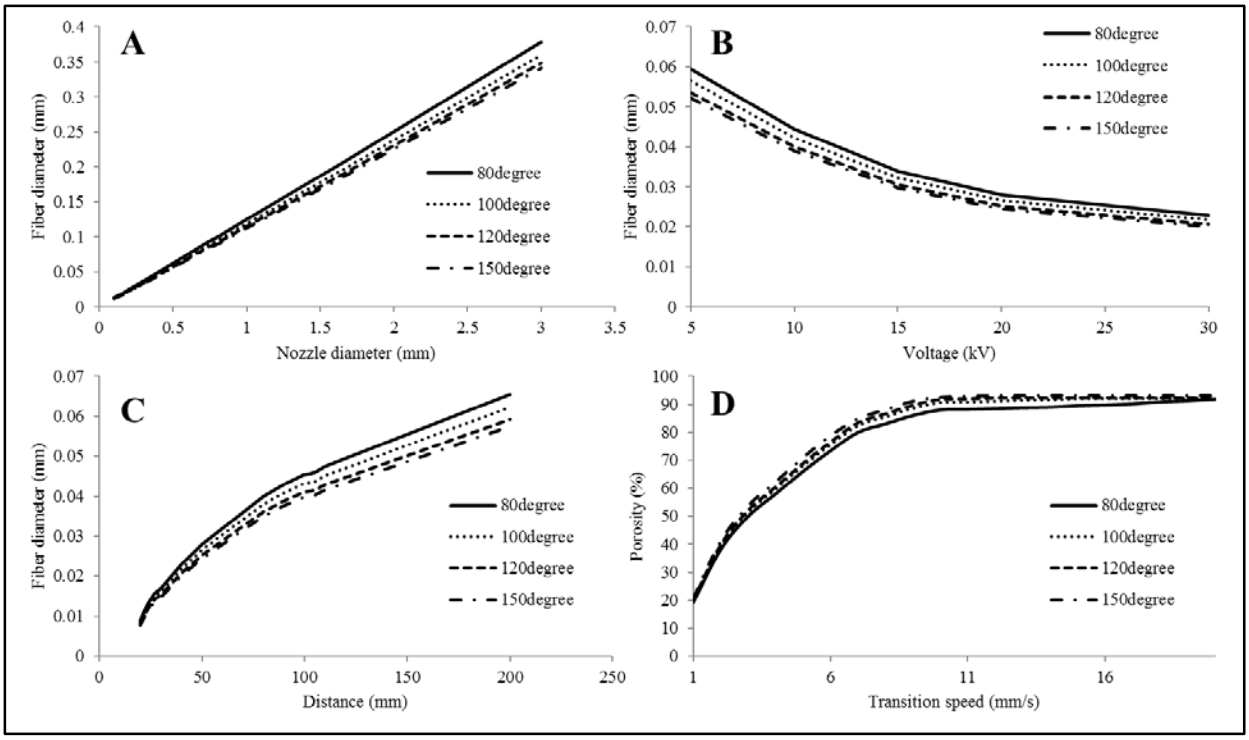

Figure 8. Predictions of fiber diameter and porosity under ambiguous conditions including various temperatures.

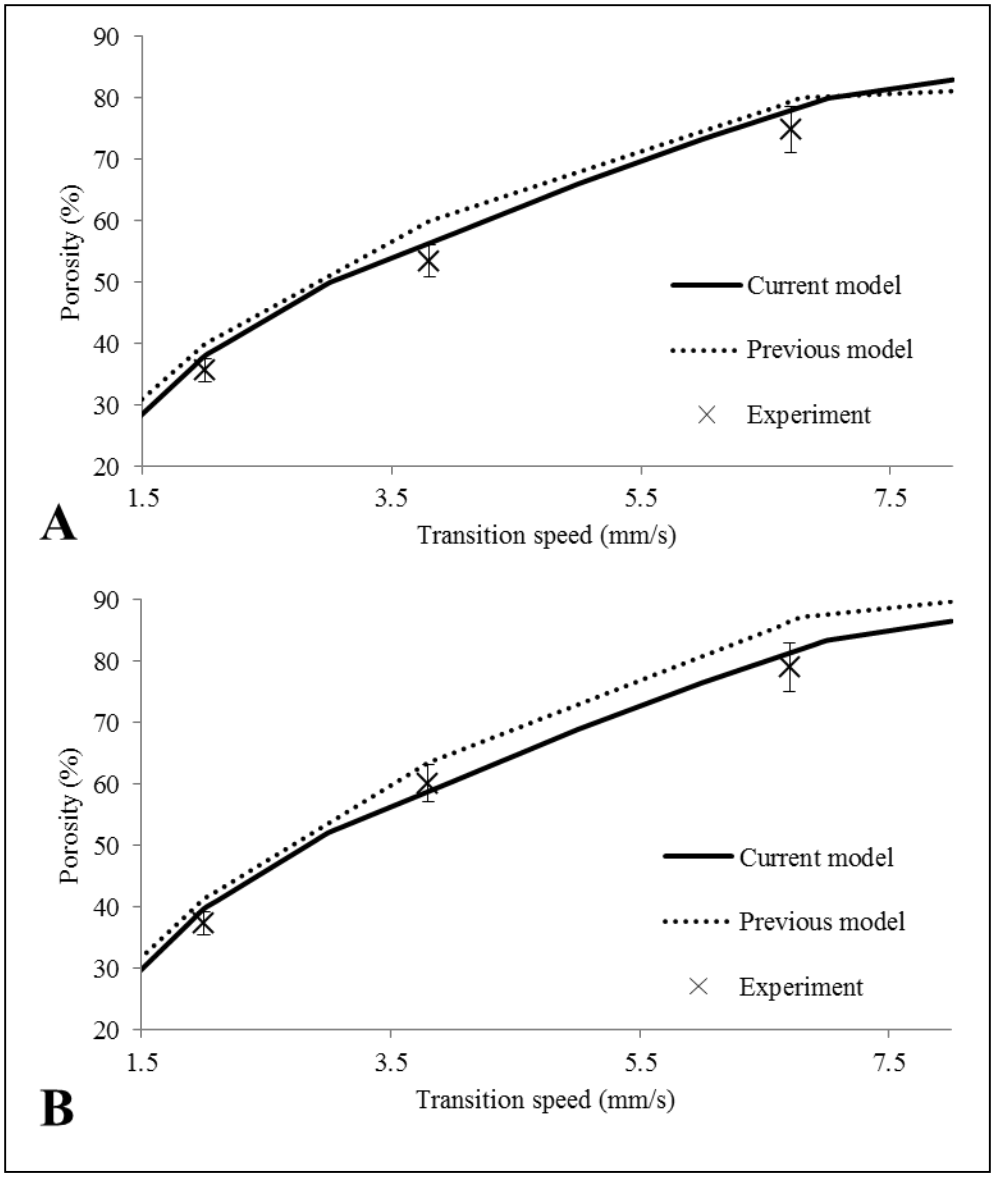

Figure 9. Comparison of porosity prediction between current model and previous model.

(A: 80˚C, B: 120 ˚C)

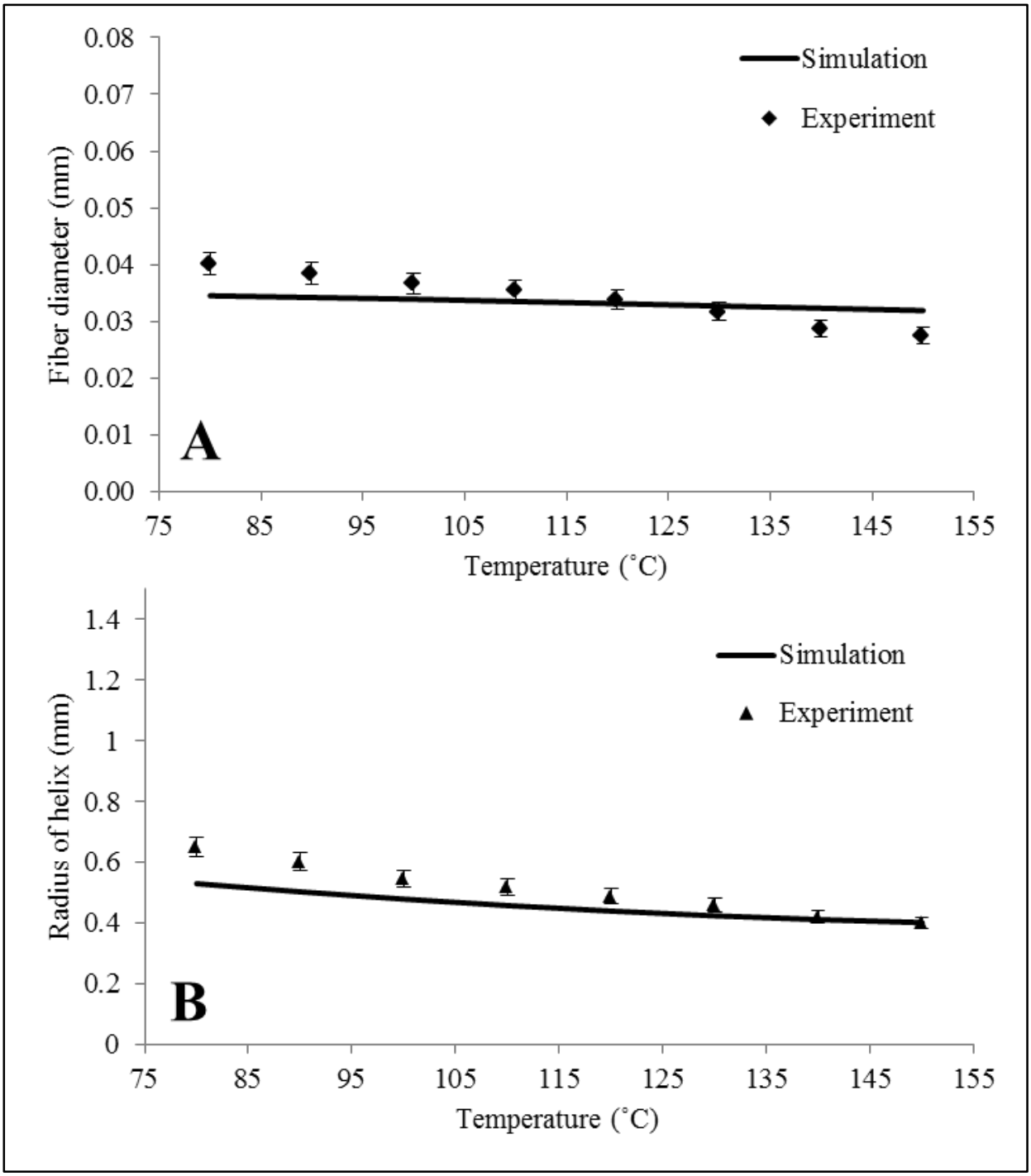

Figure 10. Results of fiber diameter (A) and radius of helix (B) controlled by temperature in simulation and experimental results. (n=5)

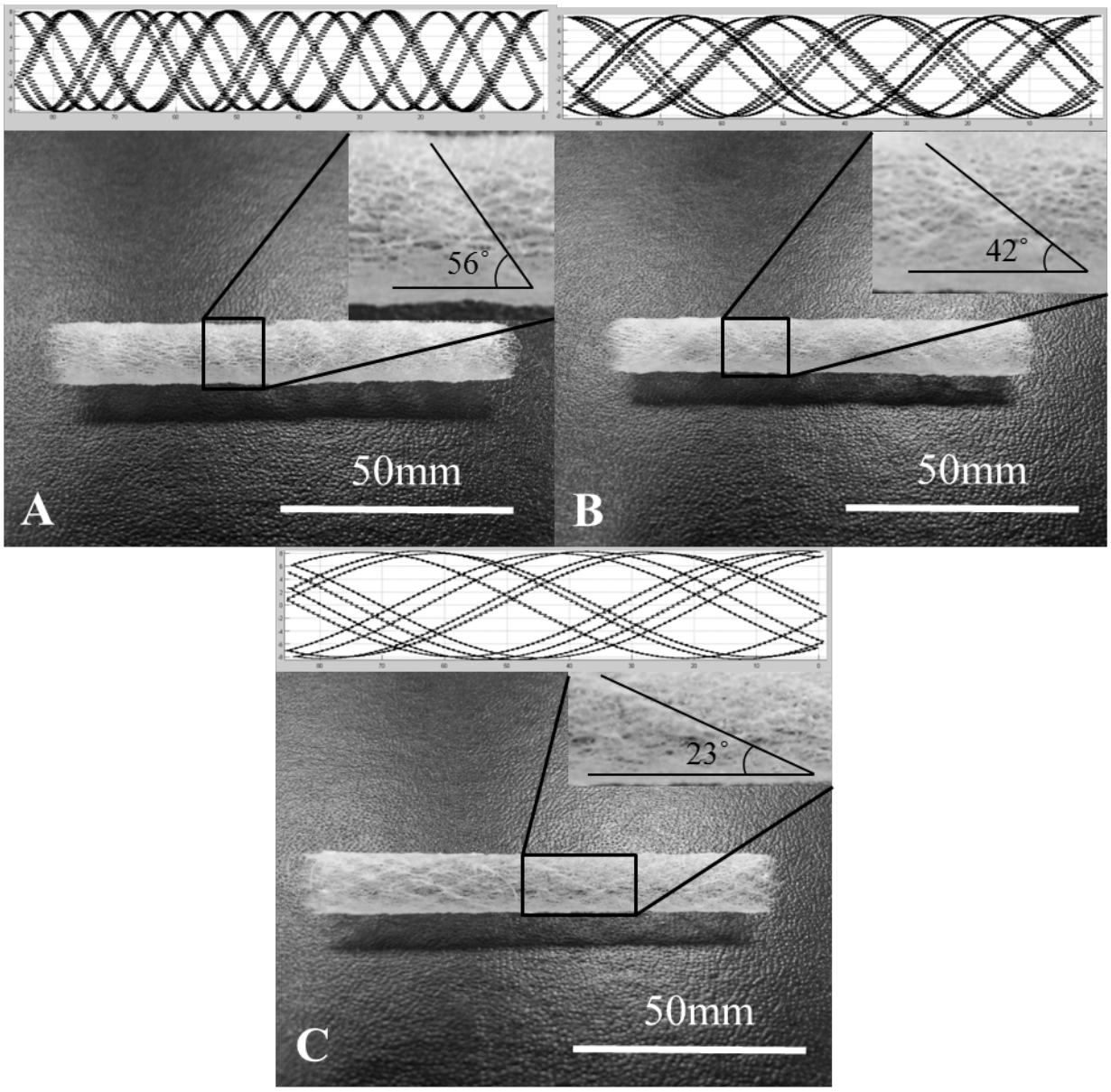

Figure 11. 3D tubular scaffold topology depended on transitional speed. (A) 4.25mm/s, (B) 8.50mm/s, (C) 17.00mm/s